

Source-Free Exchange-Correlation Magnetic Fields in Density Functional Theory

S. Sharma,*¹ E. K. U. Gross, A. Sanna, and J. K. Dewhurst

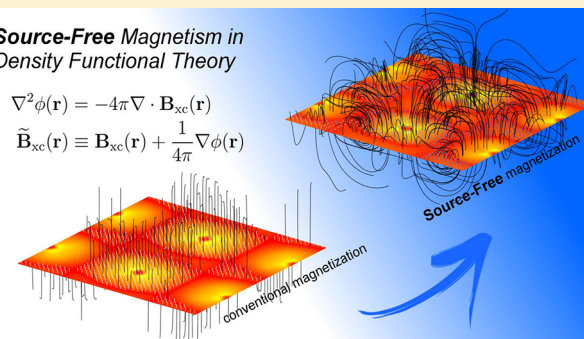
Max-Planck-Institut für Mikrostrukturphysik, Weinberg 2, D-06120 Halle, Germany

ABSTRACT: Spin-dependent exchange-correlation energy functionals in use today depend on the charge density and the magnetization density: $E_{xc}[\rho, \mathbf{m}]$. However, it is also correct to define the functional in terms of the curl of \mathbf{m} for physical external fields: $E_{xc}[\rho, \nabla \times \mathbf{m}]$. The exchange-correlation magnetic field, \mathbf{B}_{xc} , then becomes source-free. We study this variation of the theory by uniquely removing the source term from local and generalized gradient approximations to the functional. By doing so, the total Kohn–Sham moments are improved for a wide range of materials for both functionals. Significantly, the moments for the pnictides are now in good agreement with experiment. This source-free method is simple to implement in all existing density functional theory codes.

Source-Free Magnetism in Density Functional Theory

$$\nabla^2 \phi(\mathbf{r}) = -4\pi \nabla \cdot \mathbf{B}_{xc}(\mathbf{r})$$

$$\tilde{\mathbf{B}}_{xc}(\mathbf{r}) \equiv \mathbf{B}_{xc}(\mathbf{r}) + \frac{1}{4\pi} \nabla \phi(\mathbf{r})$$



1. INTRODUCTION

Density functional theory (DFT)^{1,2} has proven enormously successful for calculating the electronic structure of both molecules and solids. Lattice structures, phonon spectra, and many other properties are now routinely calculated. Magnetism presents more of a mixed picture. Simple magnets, such as elemental solids (Fe, Co, and Ni), are well-described by the local spin density approximation (LSDA)³ or the generalized gradient approximations (GGA), at least as far as total moments are concerned. However, both LSDA and GGA perform poorly for the iron pnictide and related materials^{4–7} for which they greatly overestimate the moments by factors of two or more (see Figure 1). This has been an impediment to investigating the microscopic magnetic structure,^{8–12} related response functions,¹³ and superconductivity^{14,15} of these materials with density functional methods.

Most approximate spin-dependent exchange-correlation energy functionals, $E_{xc}[\rho, \mathbf{m}]$, use the density and magnetization as their arguments.^{16–19} This form is dictated by the many-body Hamiltonian used originally in the context of spin DFT (SDFT) by von Barth and Hedin¹⁶

$$\hat{H} = \sum_{i=1} \left[-\frac{1}{2} \nabla_i^2 + V_{\text{ext}}(\mathbf{r}_i) + \vec{\sigma} \cdot \mathbf{B}_{\text{ext}}(\mathbf{r}_i) + \frac{1}{2} \sum_{j \neq i} \frac{1}{|\mathbf{r}_i - \mathbf{r}_j|} \right] \quad (1)$$

where V_{ext} and \mathbf{B}_{ext} are the external scalar potential and magnetic fields, respectively; and the sum runs to the number of particles. The external magnetic field was assumed to be an unconstrained vector field in the original formulation of SDFT. Physical magnetic fields are not unconstrained but rather the curl of a vector potential, i.e. $\mathbf{B}_{\text{ext}} = \nabla \times \mathbf{A}_{\text{ext}}$. With this constraint it is possible to demonstrate (see refs 20 and 21 and Section 2.2) that the exchange-correlation functional can be

chosen to depend on the spin current $\nabla \times \mathbf{m}(\mathbf{r})$ instead of $\mathbf{m}(\mathbf{r})$: $\tilde{E}_{xc}[\rho, \nabla \times \mathbf{m}]$.

An immediate consequence of this is that the functional derivative of $\tilde{E}_{xc}[\rho, \nabla \times \mathbf{m}]$ with respect to $\mathbf{m}(\mathbf{r})$ is of the form $\tilde{\mathbf{B}}_{xc}(\mathbf{r}) \equiv \delta \tilde{E}_{xc} / \delta \mathbf{m}(\mathbf{r}) = \nabla \times \mathbf{A}_{xc}(\mathbf{r})$ which implies $\nabla \cdot \tilde{\mathbf{B}}_{xc}(\mathbf{r}) = 0$. In other words, the exchange-correlation magnetic field is *source-free*.

Functionals in common use, such as LSDA and GGA, are not, in general, source-free. One may therefore reasonably ask how can LSDA or GGA be modified so that they do have this property, i.e. how can any approximate \mathbf{B}_{xc} be made source-free and how does this affect the magnetic properties of materials. In the present work we show a simple method of removing the source-term from any exchange-correlation density functional. We then apply this procedure to Perdew–Wang LSDA³ and PBE-GGA:²² first we enhance the strength of the exchange splitting and then modify the functional in a unique way to become source-free. These new source-free functionals are then used to study several classes of magnetic materials (elemental solids, pnictides, heuslers, etc.), and the results show that (a) the good moments of LSDA for elemental solids are retained, (b) the large overestimation of pnictide moments is cured demonstrating that this “unphysical” source term in LSDA and PBE-GGA may be responsible for a large deviation of calculated magnetic moments from experiments, and (c) the PBE-GGA now yields better results than LSDA for both classes of materials. Our implementation is publicly available in the Elk Code²³ and so can be applied to many more such materials.

Received: October 17, 2017

Published: February 8, 2018

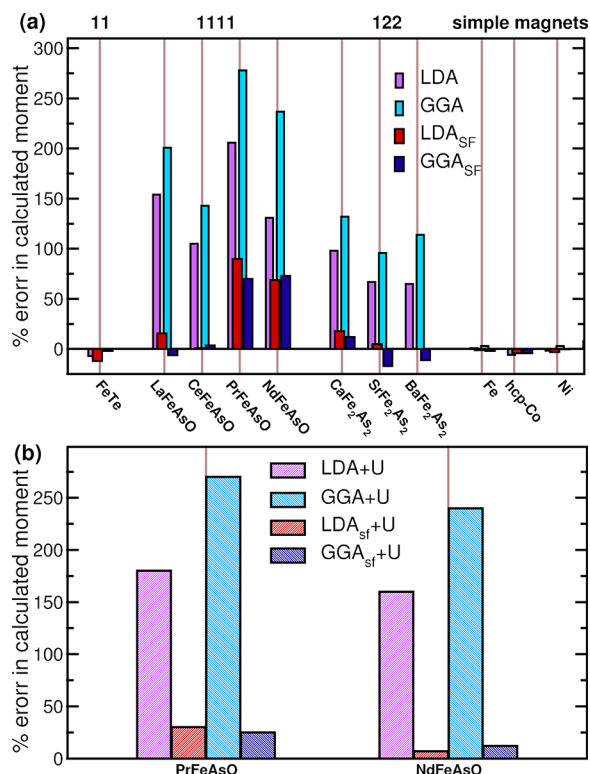


Figure 1. Percentage deviation of the calculated magnetic moment from experimental data for 11, 1111, and 122 pnictides as well as elemental solids. (a) Results calculated using LSDA (pink), GGA (PBE – cyan), and their source-free counterparts LSDA_{SF} (red) and PBE-GGA_{SF} (blue). (b) Same as (a) but by adding an on-site Coulomb repulsion U on the f -states. Root-mean-square-percentage errors are LSDA: 90.2%, PBE-GGA: 143%, LSDA_{SF}: 34%, PBE-GGA_{SF}: 31%, LSDA_{SF} + U : 16%, PBE-GGA_{SF} + U : 11%.

2. SOURCE-FREE FUNCTIONAL

In this section we first show that the exchange-correlation functional can be chosen to be source-free. Then we demonstrate how we construct a new source-free functional from existing density functionals.

2.1. Exchange-Correlation Functional Can Be Chosen Source-Free. Let

$$E[V_{\text{ext}}, B_{\text{ext}}] = \min_{|\Psi\rangle} \langle \Psi | \hat{H} | \Psi \rangle \quad (2)$$

where \hat{H} is given in eq 1, and the minimization over all N -electron states $|\Psi\rangle$ is the total energy as a functional of the external potential and magnetic field. This can be written as a constrained minimization

$$E[V_{\text{ext}}, B_{\text{ext}}] = \min_{(\rho, \mathbf{m})} \min_{|\Psi\rangle \rightarrow (\rho, \mathbf{m})} \langle \Psi | \hat{H} | \Psi \rangle \quad (3)$$

$$= \min_{(\rho, \mathbf{m})} \left\{ \int d^3r V_{\text{ext}}(\mathbf{r}) \rho(\mathbf{r}) + \int d^3r \mathbf{B}_{\text{ext}}(\mathbf{r}) \cdot \mathbf{m}(\mathbf{r}) + F[\rho, \mathbf{m}] \right\} \quad (4)$$

where

$$F[\rho, \mathbf{m}] \equiv \min_{|\Psi\rangle \rightarrow (\rho, \mathbf{m})} \langle \Psi | \hat{T} + \hat{V}_{\text{ee}} | \Psi \rangle \quad (5)$$

is a universal functional of density and magnetization; \hat{T} and \hat{V}_{ee} are the kinetic and electron–electron interaction parts of the

Hamiltonian, respectively. Likewise, the noninteracting kinetic energy functional is defined as

$$T_s[\rho, \mathbf{m}] \equiv \min_{|\Psi\rangle \rightarrow (\rho, \mathbf{m})} \langle \Psi | \hat{T} | \Psi \rangle \quad (6)$$

from which is obtained the exchange-correlation energy functional $E_{\text{xc}}[\rho, \mathbf{m}] \equiv F[\rho, \mathbf{m}] - T_s[\rho, \mathbf{m}] - E_{\text{H}}[\rho]$, where E_{H} is the usual Hartree energy.

However, if we assume that the external magnetic field is physical, i.e. $\mathbf{B}_{\text{ext}}(\mathbf{r}) = \nabla \times \mathbf{A}_{\text{ext}}(\mathbf{r})$, and the magnetization tends to zero at a large distance, then the classical energy of the external magnetic field can be written as

$$\int d^3r (\nabla \times \mathbf{A}_{\text{ext}}(\mathbf{r})) \cdot \mathbf{m}(\mathbf{r}) = \int d^3r \mathbf{A}_{\text{ext}}(\mathbf{r}) \cdot (\nabla \times \mathbf{m}(\mathbf{r})) \quad (7)$$

Thus, we can define another universal functional $\tilde{F}[\rho, \nabla \times \mathbf{m}]$ as

$$\tilde{F}[\rho, \nabla \times \mathbf{m}] \equiv \min_{|\Psi\rangle \rightarrow (\rho, \nabla \times \mathbf{m})} \langle \Psi | \hat{T} + \hat{V}_{\text{ee}} | \Psi \rangle \quad (8)$$

with analogous functionals $\tilde{T}[\rho, \nabla \times \mathbf{m}]$ and $\tilde{E}_{\text{xc}}[\rho, \nabla \times \mathbf{m}]$. On the space of densities obtained from physical external magnetic fields we have that $E_{\text{xc}}[\rho, \mathbf{m}] = \tilde{E}_{\text{xc}}[\rho, \nabla \times \mathbf{m}]$. This implies that the total energy obtained from both functionals is also the same for physical densities.

The equality of the functionals does not hold in general for densities obtained from external magnetic fields which have a source term. A consequence of this is that the unconstrained functional derivative of E_{xc} with respect to $\mathbf{m}(\mathbf{r})$ is different for the two functionals, i.e. $\mathbf{B}_{\text{xc}}(\mathbf{r}) \neq \tilde{\mathbf{B}}_{\text{xc}}(\mathbf{r})$ in general. The functional derivative of \tilde{E}_{xc} can be further evaluated as

$$\begin{aligned} \tilde{\mathbf{B}}_{\text{xc}}(\mathbf{r}) &\equiv \left. \frac{\delta \tilde{E}_{\text{xc}}[\rho, \nabla \times \mathbf{m}]}{\delta \mathbf{m}(\mathbf{r})} \right|_{\rho} \\ &= \int d^3r' \frac{\delta(\nabla \times \mathbf{m}(\mathbf{r}'))}{\delta \mathbf{m}(\mathbf{r})} \frac{\delta \tilde{E}_{\text{xc}}[\rho, \nabla \times \mathbf{m}]}{\delta(\nabla \times \mathbf{m}(\mathbf{r}'))} \bigg|_{\rho} \\ &= \int d^3r' \delta(\mathbf{r} - \mathbf{r}') \nabla \times \frac{\delta \tilde{E}_{\text{xc}}[\rho, \nabla \times \mathbf{m}]}{\delta(\nabla \times \mathbf{m}(\mathbf{r}'))} \bigg|_{\rho} \\ &= \int d^3r' \delta(\mathbf{r} - \mathbf{r}') \nabla \times \mathbf{A}_{\text{xc}}(\mathbf{r}') \\ &= \nabla \times \mathbf{A}_{\text{xc}}(\mathbf{r}) \end{aligned} \quad (9)$$

proving that $\tilde{\mathbf{B}}_{\text{xc}}$ is indeed source-free. We note that this derivation also holds for the case where \mathbf{A}_{ext} and \mathbf{m} are lattice-periodic. In this case, the surface term, which had to be zero in order to derive eq 7, sums to zero over the faces of the periodic box.

An essential aspect of this version of SDFT is that the Kohn–Sham magnetization $\mathbf{m}(\mathbf{r})$ obtained from the exact $\tilde{\mathbf{B}}_{\text{xc}}$ is not itself exact, but rather only its curl is. The difference between the two is a curl-free function which is therefore the gradient of some scalar function: $\nabla f(\mathbf{r})$. Thus, one loses some information about the magnetization by using the source-free theory but not, as it turns out, the total moment. For finite systems, the total moment obtained from the Kohn–Sham magnetization using $\tilde{\mathbf{B}}_{\text{xc}}$ is also exact because the integral of $\nabla f(\mathbf{r})$ over all space is zero. This is not true for periodic boundary conditions. In this case, the functional domain has to be augmented with the total moment vector \mathbf{M} , thus $\tilde{E}_{\text{xc}} \equiv$

Table 1. Magnetic Moment (in μ_B) per Fe Atom for Pnictides and per Magnetic Atom for the Rest of the Materials^a

material	expt	LSDA	LSDA _{sf}	PBE-GGA	PBE-GGA _{sf}
LaFeAsO ²⁹	0.63 ³⁰	1.60	0.73 (+0.1)	1.92	0.59 (−0.04)
LaFeAsO ³¹		1.39	0.7 (+0.07)	1.8	0.58 (−0.05)
LaFeAsO ³²			0.68 (+0.05)		0.56 (−0.07)
CeFeAsO ³³	0.8 ³⁴	1.64	0.81 (+0.01)	1.95	0.83 (+0.03)
PrFeAsO ³⁵	0.5 ³⁶	1.53	0.99 (+0.49)	1.89	0.85 (+0.35)
NdFeAsO ³⁷	0.54 ³⁸	1.24	0.91 (+0.37)	1.82	0.93 (+0.39)
CaFe ₂ As ₂ ³⁹	0.8 ⁴⁰	1.59	0.95 (+0.15)	1.86	0.90 (+0.1)
SrFe ₂ As ₂ ⁴¹	0.94 ⁴²	1.57	0.98 (+0.04)	1.84	0.78 (−0.16)
BaFe ₂ As ₂ ⁴³	0.87 ⁴⁴	1.43	0.87 (0.00)	1.84	0.78 (−0.09)
BaFe ₂ As ₂ ³¹		1.38	0.73 (−0.14)	1.67	0.59 (−0.28)
FeTe ⁴⁵	2.25 ⁴⁶	2.10	1.73 (−0.52)	2.25	1.85 (−0.40)
bcc-Fe	2.2	2.15	2.22 (+0.02)	2.27	2.16 (−0.04)
hcp-Co	1.7	1.63	1.60 (−0.1)	1.67	1.61 (−0.09)
Ni	0.65	0.64	0.63 (−0.02)	0.67	0.65 (0.00)
Fe ₂ CoAl	1.637	1.77	1.72 (+0.08)	1.85	1.61 (−0.03)
Ni ₃ Al	0.077	0.17	0.1225 (+0.04)	0.1825	0.1725 (+0.09)
ZrZn ₂	0.085	0.21	0.197 (+0.11)	0.283	0.257 (+0.17)

^aAbsolute error from experimental data is written in brackets. For pnictides the moment is known to be highly sensitive to the structural details; hence the references for experimental structural data are cited in the first column; and the references for magnetic moment are cited in the second column. Results are presented for one representative Heusler (Fe₂CoAl) material out of a total of 28 studied by us.

$\tilde{E}_{xc}[\rho, \nabla \times \mathbf{m}, \mathbf{M}]$. This is analogous to the macroscopic polarization required as an extra variable in the presence of an external electric field applied to a solid.²⁴ The variable conjugate to \mathbf{M} now has to be included in the calculation; this variable is clearly a constant magnetic field and corresponds to an \mathbf{A}_{ext} which diverges at large distance. In addition to \mathbf{M} the source-free approach also allows computation of the integrated moments over any region in space bounded by a zero- \mathbf{m} surface; this implies that atomic moments are also directly accessible.

2.2. Constructing the Source-Free Functional. In order to make the existing LDA or GGA functionals source-free, we appeal to Helmholtz's theorem which states that any vector field on a domain in \mathbb{R}^3 , which is twice differentiable, can be decomposed into a curl-free component and a source-free component. This decomposition is unique for given boundary conditions. Thus, let ϕ be the solution to Poisson's equation (in atomic units)

$$\nabla^2 \phi(\mathbf{r}) = -4\pi \nabla \cdot \mathbf{B}_{xc}(\mathbf{r}) \quad (10)$$

and define

$$\tilde{\mathbf{B}}_{xc}(\mathbf{r}) \equiv \mathbf{B}_{xc}(\mathbf{r}) + \frac{1}{4\pi} \nabla \phi(\mathbf{r}) \quad (11)$$

then $\nabla \cdot \tilde{\mathbf{B}}_{xc}(\mathbf{r}) = 0$, i.e. $\tilde{\mathbf{B}}_{xc}$ is source-free. It is important to note that the scalar part of the potential, $V_{xc}(\mathbf{r})$, is not directly affected by this procedure. This modified functional has certain intrinsic properties: (a) it is still correct for homogeneous electron gas (HEG) because \mathbf{B}_{xc}^{HEG} is a constant implying that $\nabla \cdot \mathbf{B}_{xc}(\mathbf{r}) = 0$, and therefore this modification has no effect, (b) since $\tilde{\mathbf{B}}_{xc}$ is obtained by solving Poisson's equation, the functional is intrinsically nonlocal, in other words, the field at \mathbf{r} depends on the magnetization everywhere, (c) $\tilde{\mathbf{B}}_{xc}$ is necessarily noncollinear, (d) in the case of unmodified LSDA/GGA, $\mathbf{m}(\mathbf{r}) \times \mathbf{B}_{xc}(\mathbf{r}) = 0$ by construction (see refs 17, 18, and 25). Removal of the source term from \mathbf{B}_{xc} results in $\mathbf{m}(\mathbf{r}) \times \tilde{\mathbf{B}}_{xc}(\mathbf{r}) \neq 0$ and hence will contribute to spin-dynamics even in the absence of the external field,²⁵ (e) the procedure is simple to implement in any DFT code since all such codes have

a Poisson equation solver, and (f) very little computational effort is needed for the modification.

We perform an additional modification of the functional which effectively enhances the spin splitting. It comprises of a simple scaling of the input magnetization $E_{xc}[\rho, \mathbf{m}] \rightarrow E_{xc}[\rho, s\mathbf{m}]$ and then a further scaling of the resultant magnetic field $\mathbf{B}_{xc} \rightarrow s\mathbf{B}_{xc}$ in order to keep the functional variational with respect to \mathbf{m} . To find the value of this scaling parameter our strategy was to choose a test set for which we find the optimal value of s , which was found to be $s = 1.12$ and $s = 1.14$ for LSDA and PBE-GGA, respectively. The same value of s is then used for the remaining materials. Our test set is comprised of two representative materials: BaFe₂As₂ and Ni. We note that this factor, though empirical, is not a material-dependent parameter. If we were to change our test set the value of the s changes; however, this change is relatively small.

At this point it is important to mention the distinction between this scaling and the one performed by Ortzen et al.,²⁶ namely (1) the present method of scaling is fully variational and (2) the value of the scaling parameter is universal (i.e., material independent). These two points make the present procedure fully self-consistent and *ab initio* in nature.

Taking a further functional derivative of eq 11, we can also compute the magnetic part of the exchange-correlation kernel, \tilde{f}_{xc} (which is a 3×3 tensor)

$$\begin{aligned} \tilde{f}_{xc}(\mathbf{r}, \mathbf{r}') &\equiv \frac{\delta^2 \tilde{E}_{xc}}{\delta \mathbf{m}(\mathbf{r}) \delta \mathbf{m}(\mathbf{r}')} = \frac{\delta \tilde{\mathbf{B}}_{xc}(\mathbf{r})}{\delta \mathbf{m}(\mathbf{r}')} \\ &= \frac{\delta \mathbf{B}_{xc}(\mathbf{r})}{\delta \mathbf{m}(\mathbf{r}')} + \frac{1}{4\pi} \frac{\delta \nabla_r \phi(\mathbf{r})}{\delta \mathbf{m}(\mathbf{r}')} \\ &= f_{xc}(\mathbf{r}, \mathbf{r}') + \int d^3 r'' M(\mathbf{r}, \mathbf{r}'') f_{xc}(\mathbf{r}'', \mathbf{r}') \end{aligned} \quad (12)$$

where we have used the explicit form of ϕ in terms of \mathbf{B}_{xc} from the formal solution of the Poisson equations,²⁷ and we have defined

$$M(\mathbf{r}, \mathbf{r}'') = \frac{1}{4\pi} \nabla_r \otimes \nabla_{r'} \frac{1}{|\mathbf{r} - \mathbf{r}''|} \quad (13)$$

3. COMPUTATIONAL DETAILS

The full potential linearized augmented plane wave (LAPW) method implemented within the Elk code²³ is used in the present work. All calculations are performed in the presence of the spin-orbit coupling. To obtain the Pauli spinor states, the Hamiltonian containing only the scalar potential is diagonalized in the LAPW basis: this is the first-variational step. The scalar states thus obtained are then used as a basis to set up a second-variational Hamiltonian with spinor degrees of freedom.²⁸ This is more efficient than simply using spinor LAPW functions, but care must be taken to ensure that there is a sufficient number of first-variational eigenstates for convergence of the second-variational problem. For example, 394 states per k-point were used for the pnictides to ensure convergence of the second variational step. We use a k-point set of $20 \times 20 \times 10$ for pnictides and $20 \times 20 \times 20$ for the rest of the materials. A smearing width of 0.027 eV was used. The technical details of the LAPW basis and the calculation of derivatives required for the source-free procedure are covered exhaustively in ref 28.

4. RESULTS

The percentage deviation in the magnetic moment from experiment is presented in Figure 1(a). We note that the magnetic moments calculated using LSDA or PBE-GGA for simple magnets (Fe, Co, and Ni) and Heuslers (in Table 1 we show results for a representative Heusler out of a set of 28 we studied) are already in very good agreement with experiment with maximum deviation of 8%. This is in contrast to the moments for pnictides which deviate strongly from experiment with a maximum error of 278%. The moments calculated using source-free LSDA and PBE-GGA are also presented in Figure 1(a) and for simple magnets they are of the same quality as that of the unmodified functionals. The fact that the integrated moments are the same does not necessarily imply that the magnetization densities are similar at each point in space. However, we find that for the simple magnets the two densities are fairly close at each point in space. In the case of pnictides, the moments show dramatic improvement. At a first glance it appears that LSDA_{SF}/PBE-GGA_{SF} substantially reduces the Fe moment for all pnictides compared to the corresponding LSDA/PBE-GGA value. A closer inspection, however, reveals that this reduction is, as it should be, highly selective in that the moment in SrFe₂As₂ is reduced by ~30% while on LaFeAsO by ~60% compared to the LSDA/PBE-GGA results. The maximum deviation is now less than 25% for all materials with the exception of NdFeAsO and PrFeAsO (see Table 1). These results indicate that one of the major reasons for the bad performance of LDA/PBE-GGA for pnictides could be the presence of large source-terms in these functionals.

For NdFeAsO and PrFeAsO the source-free functionals provide a considerable improvement over unmodified LSDA or PBE-GGA, but the percentage deviation from experiment is still relatively large. We find the reason behind this to be the moment on the strongly correlated rare earth atoms. In these materials the moment of the rare-earth atom is known to be strongly coupled to the moment on the Fe atoms,³⁸ and the rare earth moment is not accurately described by the source-free functional alone.⁴⁸ In order to treat these, we use the well-established method⁴⁹ of applying an on-site Coulomb repulsion

U . It is important to mention that U was applied only to the f -states of the rare-earth atom and chosen to reproduce the experimental moment of that atom only. Nevertheless, this substantially improves the moment on the Fe sites (see Table 2). Like experiments we find the moment on rare-earths to be in-plane and oriented perpendicular to the moment on the Fe atoms.

Table 2. Magnetic Moment (in μ_B) per Atom^a

material	expt	LSDA	PBE-GGA	LSDA _{SF}	PBE-GGA _{SF}
PrFeAsO	Fe: 0.5	1.40	1.9	0.65	0.63
	Pr: 0.87	0.30	0.30	0.81	0.83
NdFeAsO	Fe: 0.54	1.42	1.84	0.50	0.61
	Nd: 0.9	2.44	1.25	0.80	0.89

^aCalculations are performed using LSDA + U , PBE-GGA + U , LSDA_{SF} + U , and PBE-GGA_{SF} + U . The values of U and J used for these calculations are given in ref 47.

The effect of the source-free functional is particularly apparent in these cases since without it the correct moment on either atom cannot be obtained for any choice of U . These results are an indication that the failure of DFT+ U in the case of pnictides may be due to the presence of source fields in the DFT functionals.

A material that also requires special attention is LaFeAsO, perhaps the most studied pnictide of all. Reported experimental values of the magnetic moment range from $0.36 \mu_B$ ⁵⁰ to $0.8 \mu_B$ ⁵¹ making it difficult to know to what our theoretical results should be compared. Perhaps the best choice is with the more recent experimental value which lies in between these two extremes, $0.63 \mu_B$.³⁰ This experiment was performed at low temperature (2 K) which is closest to our theoretical ideal of zero temperature. Another reasonable choice would be $0.8 \mu_B$ ⁵¹ since, like our theoretical work, these experiments are performed on single crystals. In either case, our results with source-free functionals still show a maximum deviation of 25%.

In the case of FeTe, the source-free functionals do not show an improvement. Experimentally FeTe is always slightly doped (with excess Fe), and describing it with the stoichiometric unit cell, as done in our work, might be one of the reasons for underestimation of the magnetic moment.

Although the source-free functional is a potential functional (see eq 12), the forces can still be calculated by using the Hellman-Feynman theorem, which requires only the charge density and the position of the nuclei. We have done so for LaOFeAs and BaFe₂As₂, and we find that the position of the As atom is within the accuracy of 0.7% which is almost the same as in the case of PBE-GGA (results for the calculated moment are presented in Table 1). The reason for this lies in the fact that the procedure of making a functional source-free affects only the \mathbf{B}_{xc} and not, directly, the Kohn-Sham scalar potential. Although, via the self-consistent procedure the density and the scalar potential also get affected but only weakly. Hence this does not significantly modify any property which depends upon the charge density alone, and the good quality of unmodified LSDA/GGA functionals is retained for such properties.

A means of summarizing the overall quality of results is the root-mean-square percentage error (RMSPE) which one expects to be reduced on improving the functional, by going, for example, from LSDA to the more sophisticated GGA. To the contrary, the value of RMSPE for LSDA is 90.2% and for PBE-GGA is 143%, i.e. the quality of results deteriorates on

improving the functional by adding gradients. These errors are greatly reduced to 34.3% with LSDA_{SF} and 30.6% with PBE-GGA_{SF}. Furthermore, once the LSDA_{SF} + *U* and PBE-GGA_{SF} + *U* results are considered, the RMSPE are 16% for source-free LSDA and 11% for source-free PBE-GGA, indicating that removal of the source term results in GGA_{SF} performing better than LSDA_{SF}.

Note that the two steps which comprise this method (i.e., scaling and making the functional source-free) must be performed in combination. Each step if applied alone yields unreasonable results (see Table 3). We found that the purely

Table 3. Magnetic Moment (in μ_B) per Fe Atom for Pnictides and per Magnetic Atom for the Rest of the Materials^a

material	expt	LSDA _s	LSDA no source	PBE-GGA _s	PBE-GGA no source
LaFeAsO	0.63	2.11	0.07	2.42	0.06
CeFeAsO	0.8	2.12	0.02	2.37	0.01
PrFeAsO	0.5	2.30	0.15	2.40	0.12
NdFeAsO	0.54	2.20	0.32	2.43	0.30
CaFe ₂ As ₂	0.8	2.20	0.07	2.46	0.06
SrFe ₂ As ₂	0.94	2.24	0.06	2.50	0.04
BaFe ₂ As ₂	0.87	2.40	0.06	2.51	0.05
FeTe	2.25	2.60	0.88	2.67	0.95
bcc-Fe	2.2	2.62	1.91	2.66	1.90
hcp-Co	1.7	1.82	1.28	1.87	1.35
Ni	0.65	0.71	0.53	0.69	0.57
Ni ₃ Al	0.077	0.26	0.01	0.29	0.06
ZrZn ₂	0.085	0.27	0.17	0.36	0.20

^aLSDA_s/GGA_s moments are calculated by enhancing the LSDA, PBE-GGA magnetization density by 1.12 and 1.14, respectively. LSDA/GGA no source results are obtained by making LSDA/PBE-GGA source free (i.e. without any scaling).

source-free LSDA and PBE-GGA functionals lead to highly underestimated moments (see Table 3). This is due to suppression of the *z*-projected moment. The magnetization density obtained by purely source-free LSDA and PBE-GGA is also highly noncollinear (i.e., *x* and *y* projected moments are as

significant as M_z). The scaling alone of the LSDA/GGA has, as expected, a rather trivial effect of increasing the moment universally since the whole $\mathbf{m}(\mathbf{r})$ is uniformly scaled. One could envisage using the scaling parameter so as to reproduce experimental moment for the materials. This, however, has the disadvantage that the scaling parameter is then functional and material-dependent e.g. $s = 1.07$ for Ni, $s = 0.91$ for LaOFeAs, and $s = 0.95$ for SrFe₂As₂ (note that purely LSDA results correspond to $s = 1$). This combination of the scaling and removing the source term leads to good agreement with experiments for a wide set of materials. Most importantly, we find that the choice of the scaling parameter is material independent and depends instead on the functional approximation class; i.e. whether the functional is a LSDA or GGA. Tests performed by fixing the value of $s = 1.14$ for various GGAs (PW91, RevPBE, PBESol, and AM05) show that the results differ from each other by a maximum of $\pm 4\%$.

At this point it is appropriate to point the limitations of the source-free functional: (1) As mentioned earlier, the correlations in the source-free functional are not sufficient for treating strongly correlated materials like rare earth magnets. (2) For Ni₃Al and ZnZr₂, even though the source-free functionals show an improvement over LDA/PBE-GGA, the percentage deviation from experiments stays large (see Table 1). This is indicative of the fact that for these two materials the presence of source-term in LDA/PBE-GGA is not the reason for their bad performance. These materials have very small moments; it is believed that spin-fluctuations have significant contribution to the physics^{52,53} even away from a quantum critical point, and this could be one of the main reasons for deviation of calculated moments from experiments.

It is enlightening to see how \mathbf{B}_{xc} of LSDA and PBE-GGA and their new source-free versions differ spatially. We plot this for the case of BaFe₂As₂ in Figure 2. It is evident from the direction of \mathbf{B}_{xc} (see arrows in figure) that removal of the source-term enhances the noncollinearity. More importantly, the field lines for LSDA are unphysical in the sense that they begin and end at different points, whereas the source-free field lines are always closed. This means that they have to follow more complicated paths in the crystal, a fact evident from Figure 2. Furthermore, we note that this source term in LSDA/PBE-GGA for

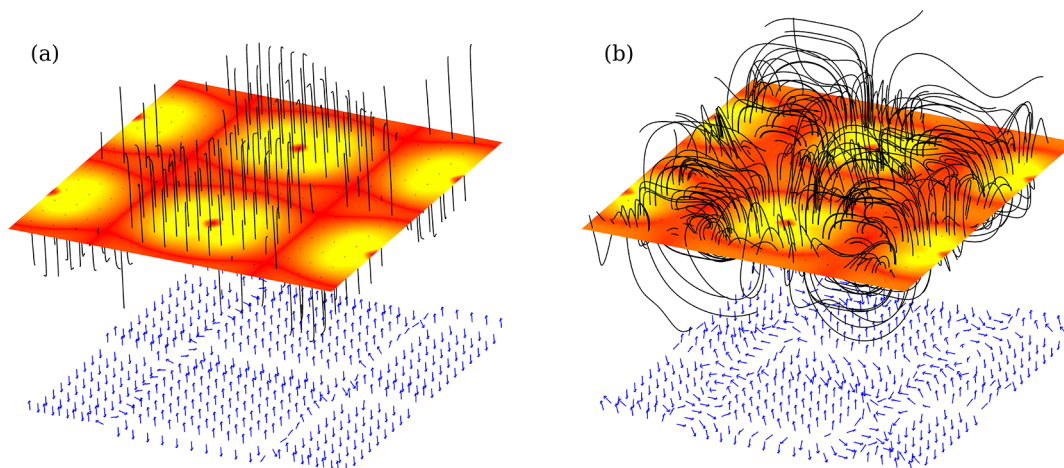


Figure 2. Vector field \mathbf{B}_{xc} for BaFe₂As₂ projected in a plane containing Fe atoms. Plot (a) is LSDA, and plot (b) is source-free LSDA. The colored plane shows the magnitude of \mathbf{B}_{xc} , and the arrows indicate the direction. The black field lines originate from a regular grid in the plane and follow the vector field. LSDA field lines show a plane of magnetic monopoles, while making LSDA source-free leads to more complicated but physical field lines. The arrows indicate that the removal of the source term leads to enhancement of noncollinearity.

elemental magnets is very small but significantly large for pnictides, and hence removal of it then leads to improved magnetic moments.

5. SUMMARY

Motivated by an exact property of spin current DFT, we removed the source term from the B_{xc} of LSDA and GGA. The spin splitting was also enhanced by a simple scaling of the input magnetization and output field. The resulting functionals were found to produce moments which were in better agreement with experiment. This improvement was particularly pronounced for the pnictides where errors were reduced from 100 to 200% down to 25% or less. Furthermore, we find that any property which depends upon the charge density alone does not significantly change by making the functional source-free, and the good quality of unmodified LSDA/GGA functionals is retained for such properties. We hope that our findings will spur the development of exchange-correlation energy functionals whose resultant magnetic fields are manifestly source-free.

AUTHOR INFORMATION

Corresponding Author

*E-mail: sharma@mpi-halle.mpg.de.

ORCID

S. Sharma: 0000-0001-8929-9376

Notes

The authors declare no competing financial interest.

ACKNOWLEDGMENTS

The authors would like to thank Kieron Burke and Carsten Ullrich for useful discussions.

REFERENCES

- (1) Hohenberg, P.; Kohn, W. Inhomogeneous Electron Gas. *Phys. Rev.* **1964**, *136*, B864.
- (2) Kohn, W.; Sham, L. J. Self-Consistent Equations Including Exchange and Correlation Effects. *Phys. Rev.* **1965**, *140*, A1133.
- (3) Perdew, J. P.; Wang, Y. Accurate and simple analytic representation of the electron-gas correlation energy. *Phys. Rev. B: Condens. Matter Mater. Phys.* **1992**, *45*, 13244.
- (4) Dai, P. Antiferromagnetic order and spin dynamics in iron-based superconductors. *Rev. Mod. Phys.* **2015**, *87*, 855.
- (5) Mazin, I. I. Perspective Article Superconductivity gets an iron boost. *Nature* **2010**, *464*, 183.
- (6) Kordyuk, A. A. Iron-based superconductors: Magnetism, superconductivity, and electronic structure (Review Article). *Low Temp. Phys.* **2012**, *38*, 888–899.
- (7) Dai, P.; Hu, J.; Dagotto, E. Magnetism and its microscopic origin in iron-based high-temperature superconductors. *Nat. Phys.* **2012**, *8*, 709–718.
- (8) Yildirim, T. Origin of the 150-K Anomaly in LaFeAsO: Competing Antiferromagnetic Interactions, Frustration, and a Structural Phase Transition. *Phys. Rev. Lett.* **2008**, *101*, 057010.
- (9) Singh, D. J.; Du, M.-H. Density Functional Study of LaFeAsO_{1-x}F_x: A Low Carrier Density Superconductor Near Itinerant Magnetism. *Phys. Rev. Lett.* **2008**, *100*, 237003.
- (10) Ma, F.; Lu, Z.-Y.; Xiang, T. Arsenic-bridged antiferromagnetic superexchange interactions in LaFeAsO. *Phys. Rev. B: Condens. Matter Mater. Phys.* **2008**, *78*, 224517.
- (11) Sharma, S.; Shallcross, S.; Dewhurst, J. K.; Sanna, A.; Bersier, C.; Massidda, S.; Gross, E. K. U. Magnetism in CeFeAsO_{1-x}F_x and LaFeAsO_{1-x}F_x from first principles. *Phys. Rev. B: Condens. Matter Mater. Phys.* **2009**, *80*, 184502.

(12) Ortenzi, L.; Gretarsson, H.; Kasahara, S.; Matsuda, Y.; Shibauchi, T.; Finkelstein, K. D.; Wu, W.; Julian, S. R.; Kim, Y.-J.; Mazin, I. I.; Boeri, L. Structural Origin of the Anomalous Temperature Dependence of the Local Magnetic Moments in the CaFe₂As₂ Family of Materials. *Phys. Rev. Lett.* **2015**, *114*, 047001.

(13) Essenberg, F.; Buczek, P.; Ernst, A.; Sandratskii, L.; Gross, E. K. U. Paramagnons in FeSe close to a magnetic quantum phase transition: Ab initio study. *Phys. Rev. B: Condens. Matter Mater. Phys.* **2012**, *86*, 060412.

(14) Mazin, I. I.; Singh, D. J.; Johannes, M. D.; Du, M. H. Unconventional Superconductivity with a Sign Reversal in the Order Parameter of LaFeAsO_{1-x}F_x. *Phys. Rev. Lett.* **2008**, *101*, 057003.

(15) Lischner, J.; Bazhurov, T.; MacDonald, A. H.; Cohen, M. L.; Louie, S. G. First-principles theory of electron-spin fluctuation coupling and superconducting instabilities in iron selenide. *Phys. Rev. B: Condens. Matter Mater. Phys.* **2015**, *91*, 020502.

(16) von Barth, U.; Hedin, L. A local exchange-correlation potential for the spin polarized case. i. *J. Phys. C: Solid State Phys.* **1972**, *5*, 1629.

(17) Sandratskii, L. M.; Guletskii, P. G. Symmetrised method for the calculation of the band structure of noncollinear magnets. *J. Phys. F: Met. Phys.* **1986**, *16*, L43.

(18) Kubler, J.; Hock, K. H.; Sticht, J.; Williams, A. R. Density functional theory of non-collinear magnetism. *J. Phys. F: Met. Phys.* **1988**, *18*, 469.

(19) Gidopoulos, N. I. Potential in spin-density-functional theory of noncollinear magnetism determined by the many-electron ground state. *Phys. Rev. B: Condens. Matter Mater. Phys.* **2007**, *75*, 134408.

(20) Eschrig, H.; Seifert, G.; Ziesche, P. Current density functional theory of quantum electrodynamics. *Solid State Commun.* **1985**, *56*, 777.

(21) Capelle, K.; Gross, E. K. U. Spin-Density Functionals from Current-Density Functional Theory and Vice Versa: A Road towards New Approximations. *Phys. Rev. Lett.* **1997**, *78*, 1872.

(22) Perdew, J. P.; Burke, K.; Ernzerhof, M. Generalized Gradient Approximation Made Simple. *Phys. Rev. Lett.* **1997**, *78*, 1396.

(23) <http://elk.sourceforge.net> (accessed Feb 12, 2018).

(24) Gonze, X.; Ghosez, P.; Godby, R. W. Density-Polarization Functional Theory of the Response of a Periodic Insulating Solid to an Electric Field. *Phys. Rev. Lett.* **1995**, *74*, 4035–4038.

(25) Sharma, S.; Dewhurst, J. K.; Ambrosch-Draxl, C.; Kurth, S.; Helbig, N.; Pittalis, S.; Shallcross, S.; Nordström, L.; Gross, E. K. U. First-Principles Approach to Noncollinear Magnetism: Towards Spin Dynamics. *Phys. Rev. Lett.* **2007**, *98*, 196405.

(26) Ortenzi, L.; Mazin, I. I.; Blaha, P.; Boeri, L. Accounting for spin fluctuations beyond local spin density approximation in the density functional theory. *Phys. Rev. B: Condens. Matter Mater. Phys.* **2012**, *86*, 064437.

(27) Arfken, G. B.; Weber, H. J. *Mathematical Methods for Physicists*; Academic Press: 2001; Chapter 1, p 101.

(28) Singh, D. J.; Nordström, L. *Planewaves Pseudopotentials and the LAPW Method*; Springer: New York, 2006; DOI: 10.1007/978-0-387-29684-5.

(29) Sefat, A. S.; Huq, A.; McGuire, M. A.; Jin, R.; Sales, B. C.; Mandrus, D.; Cranswick, L. M. D.; Stephens, P. W.; Stone, K. H. Superconductivity in LaFe_{1-x}Co_xAsO. *Phys. Rev. B: Condens. Matter Mater. Phys.* **2008**, *78*, 104505.

(30) Qureshi, N.; Drees, Y.; Werner, J.; Wurmehl, S.; Hess, C.; Klingeler, R.; Büchner, B.; Fernández-Díaz, M. T.; Braden, M. Crystal and magnetic structure of the oxypnictide superconductor LaFeAsO_{1-x}F_x: A neutron-diffraction study. *Phys. Rev. B: Condens. Matter Mater. Phys.* **2010**, *82*, 184521.

(31) The PBE optimized lattice parameters for LaOFeAs are $a = 5.693$ Å, $b = 5.761$ Å, $c = 8.705$ Å, and $Z_{As} = 0.64608$, and the PBE optimized lattice parameters for BaFe₂As₂ are $a = 5.61$ Å, $b = 5.707$ Å, $c = 12.872$ Å, and $Z_{As} = 0.6497$.

(32) The source-free PBE optimized $Z_{As} = 0.6458$ for LaOFeAs.

(33) Zhao, J.; Huang, Q.; de la Cruz, C.; Li, S.; Lynn, J. W.; Chen, Y.; Green, M. A.; Chen, G. F.; Li, G.; Li, Z.; Luo, J. L.; Wang, N. L.; Dai, P. Structural and magnetic phase diagram of CeFeAsO_{1-x}F_x and its

relation to high-temperature superconductivity. *Nat. Mater.* **2008**, *7*, 953.

(34) Zhang, Q.; Tian, W.; Li, H.; Kim, J.-W.; Yan, J.; McCallum, R. W.; Lograsso, T. A.; Zarestky, J. L.; Bud'ko, S. L.; McQueeney, R. J.; Vagnin, D. Magnetic structures and interplay between rare-earth Ce and Fe magnetism in single-crystal CeFeAsO. *Phys. Rev. B: Condens. Matter Mater. Phys.* **2013**, *88*, 174517.

(35) Zhao, J.; Huang, Q.; de la Cruz, C.; Lynn, J. W.; Lumsden, M. D.; Ren, Z. A.; Yang, J.; Shen, X.; Dong, X.; Zhao, Z.; Dai, P. Lattice and magnetic structures of PrFeAsO, PrFeAsO_{0.85}F_{0.15}, and PrFeAsO_{0.85}. *Phys. Rev. B: Condens. Matter Mater. Phys.* **2008**, *78*, 132504.

(36) Kimber, S. A. J.; Argyriou, D. N.; Yokaichiya, F.; Habicht, K.; Gerischer, S.; Hansen, T.; Chatterji, T.; Klingeler, R.; Hess, C.; Behr, G.; Kondrat, A.; Büchner, B. Magnetic ordering and negative thermal expansion in PrFeAsO. *Phys. Rev. B: Condens. Matter Mater. Phys.* **2008**, *78*, 140503.

(37) Qiu, Y.; Bao, W.; Huang, Q.; Yildirim, T.; Simmons, J. M.; Green, M. A.; Lynn, J. W.; Gasparovic, Y. C.; Li, J.; Wu, T.; Wu, G.; Chen, X. H. Crystal Structure and Antiferromagnetic Order in NdFeAsO_{1-x}F_x ($x = 0.0$ and 0.2) Superconducting Compounds from Neutron Diffraction Measurements. *Phys. Rev. Lett.* **2008**, *101*, 257002.

(38) Tian, W.; Ratcliff, W.; Kim, M. G.; Yan, J.-Q.; Kienzle, P. A.; Huang, Q.; Jensen, B.; Dennis, K. W.; McCallum, R. W.; Lograsso, T. A.; McQueeney, R. J.; Goldman, A. I.; Lynn, J. W.; Kreyssig, A. Interplay of Fe and Nd magnetism in NdFeAsO single crystals. *Phys. Rev. B: Condens. Matter Mater. Phys.* **2010**, *82*, 060514.

(39) Kreyssig, A.; et al. Pressure-induced volume-collapsed tetragonal phase of CaFe₂As₂ as seen via neutron scattering. *Phys. Rev. B: Condens. Matter Mater. Phys.* **2008**, *78*, 184517.

(40) Goldman, A. I.; Argyriou, D. N.; Ouladdiaf, B.; Chatterji, T.; Kreyssig, A.; Nandi, S.; Ni, N.; Bud'ko, S. L.; Canfield, P. C.; McQueeney, R. J. Lattice and magnetic instabilities in CaFe₂As₂: A single-crystal neutron diffraction study. *Phys. Rev. B: Condens. Matter Mater. Phys.* **2008**, *78*, 100506.

(41) Tegel, M.; Rotter, M.; Weiss, V.; Schappacher, F. M.; Pöttgen, M. A.; Johrendt, D. Structural and magnetic phase transitions in the ternary iron arsenides SrFe₂As₂ and EuFe₂As₂. *J. Phys.: Condens. Matter* **2008**, *20*, 452201.

(42) Zhao, J.; Ratcliff, W.; Lynn, J. W.; Chen, G. F.; Luo, J. L.; Wang, N. L.; Hu, J.; Dai, P. Spin and lattice structures of single-crystalline SrFe₂As₂. *Phys. Rev. B: Condens. Matter Mater. Phys.* **2008**, *78*, 140504.

(43) Mittal, R.; Mishra, S. K.; Chaplot, S. L.; Ovsyannikov, S. V.; Greenberg, E.; Trots, D. M.; Dubrovinsky, L.; Su, Y.; Brueckel, T.; Matsuishi, S.; Hosono, H.; Garbarino, G. Ambient- and low-temperature synchrotron x-ray diffraction study of BaFe₂As₂ and CaFe₂As₂ at high pressures up to 56 GPa. *Phys. Rev. B: Condens. Matter Mater. Phys.* **2011**, *83*, 054503.

(44) Huang, Q.; Qiu, Y.; Bao, W.; Green, M. A.; Lynn, J. W.; Gasparovic, Y. C.; Wu, T.; Wu, G.; Chen, X. H. Neutron-Diffraction Measurements of Magnetic Order and a Structural Transition in the Parent BaFe₂As₂ Compound of FeAs-Based High-Temperature Superconductors. *Phys. Rev. Lett.* **2008**, *101*, 257003.

(45) Caglieri, F.; Ricci, F.; Lamura, G.; Martinelli, A.; Palenzona, A.; Pallecchi, I.; Sala, A.; Profeta, G.; Putti, M. Theoretical and experimental investigation of magnetotransport in iron chalcogenides. *Sci. Technol. Adv. Mater.* **2012**, *13*, 054402.

(46) Li, S.; de la Cruz, C.; Huang, Q.; Chen, Y.; Lynn, J. W.; Hu, J.; Huang, Y.-L.; Hsu, F.-C.; Yeh, K.-W.; Wu, M.-K.; Dai, P. First-order magnetic and structural phase transitions in Fe_{1+y}Se_xTe_{1-x}. *Phys. Rev. B: Condens. Matter Mater. Phys.* **2009**, *79*, 054503.

(47) The values of U and J used with the LSDA functional are $U = 2.04$ eV, $J = 0.57$ eV for NdFeAsO and $U = 3.27$ eV, $J = 0.67$ eV for PrFeAsO. The values used in combination of GGA are $U = 4.7$ eV, $J = 1.4$ eV for NdFeAsO and $U = 2.04$ eV, $J = 1.15$ eV for PrFeAsO.

(48) Moment for the Pr atom: LSDA_{SF} = $1.67 \mu_B$, GGA_{SF} = $1.8 \mu_B$ and for the Nd atom: LSDA_{SF} = $2.9 \mu_B$, GGA_{SF} = $2.9 \mu_B$.

(49) Liechtenstein, A. I.; Anisimov, V. I.; Zaanen, J. Density-functional theory and strong interactions: Orbital ordering in Mott-

Hubbard insulators. *Phys. Rev. B: Condens. Matter Mater. Phys.* **1995**, *52*, R5467.

(50) de la Cruz, C.; Huang, Q.; Lynn, J. W.; Li, J.; Ratcliff, W.; Zarestky, J. L.; Mook, H. A.; Chen, G. F.; Luo, J. L.; Wang, N. L.; Dai, P. Magnetic order close to superconductivity in the iron-based layered LaO_{1-x}F_xFeAs systems. *Nature* **2008**, *453*, 899.

(51) Li, H.-F.; Tian, W.; Yan, J.-Q.; Zarestky, J. L.; McCallum, R. W.; Lograsso, T. A.; Vagnin, D. Phase transitions and iron-ordered moment form factor in LaFeAsO. *Phys. Rev. B: Condens. Matter Mater. Phys.* **2010**, *82*, 064409.

(52) Aguayo, A.; Mazin, I. I.; Singh, D. J. Why Ni₃Al Is an Itinerant Ferromagnet but Ni₃Ga Is Not. *Phys. Rev. Lett.* **2004**, *92*, 147201.

(53) Singh, D. J.; Mazin, I. I. Competition of Spin Fluctuations and Phonons in Superconductivity of ZrZn₂. *Phys. Rev. Lett.* **2002**, *88*, 187004.